
Hyperparameter Sensitivity in Deep Outlier Detection Analysis and a Scalable Hyper-Ensemble Solution

Xueying Ding

Heinz College of Information Systems
Carnegie Mellon University
xding2@andrew.cmu.edu

Lingxiao Zhao

Heinz College of Information Systems
Carnegie Mellon University
lingxiao@cmu.edu

Leman Akoglu

Heinz College of Information Systems
Carnegie Mellon University
lakoglu@andrew.cmu.edu

Abstract

Outlier detection (OD) literature exhibits numerous algorithms as it applies to diverse domains. However, given a new detection task, it is unclear how to choose an algorithm to use, nor how to set its hyperparameter(s) (HPs) in unsupervised settings. HP tuning is an ever-growing problem with the arrival of many new detectors based on deep learning. While they have appealing properties such as task-driven representation learning and end-to-end optimization, deep models come with a long list of HPs. Surprisingly, the issue of model selection in the outlier mining literature has been “the elephant in the room”; a significant factor in unlocking the utmost potential of deep methods, yet little said or done to systematically tackle the issue. In the first part of this paper, we conduct the first large-scale analysis on the HP sensitivity of deep OD methods, and through more than 35,000 trained models, quantitatively demonstrate that model selection is inevitable. Next, we design a HP-robust and scalable deep *hyper-ensemble* model called ROBOD that assembles models with varying HP configurations, bypassing the choice paralysis. Importantly, we introduce novel strategies to speed up ensemble training, such as parameter sharing, batch/simultaneous training, and data subsampling, that allow us to train fewer models with fewer parameters. Extensive experiments on both image and tabular datasets show that ROBOD achieves and retains robust, state-of-the-art detection performance as compared to its modern counterparts, while taking only 2-10% of the time by the naïve hyper-ensemble with independent training.

1 Introduction

Outlier detection (OD) finds numerous real-world applications in finance, security, healthcare, to name a few. Thanks to this popularity, the literature has grown to offer a large catalog of detection algorithms [1]. With the recent advances in deep learning, the literature has been booming with the addition of many more OD models based on deep neural networks (NNs). (See surveys [30, 34, 9].)

While there is no shortage of OD methods today, given a new task, it is unclear how to choose which algorithm or model to use, nor how to configure its hyperparameter(s) (HPs) in unsupervised settings. That is, the fundamental problem of outlier model selection remains vastly understudied. Several evaluation studies have illustrated the sensitivity to HPs for traditional (i.e. non-deep) OD methods [2, 17, 8]. Most surprisingly, however, the issue of HP tuning/model selection for the newly

burgeoning deep OD models has been “the elephant in the room”; a well-known problem that no one seems to want to bring up, which is exactly the focus of this paper.

Deep OD models are promising thanks to appealing properties such as task-driven representation learning and end-to-end optimization. On the other hand, while their traditional counterparts had only 1-2 HPs¹, deep OD models come with a long list of HPs: (i) architecture HPs (e.g. depth, width), (ii) regularization HPs (e.g. dropout, weight decay rates), and (iii) optimization HPs (e.g. learning rate, epochs). These are inherited ones from regular deep NNs while most also exhibit their model-specific/specialized HPs. It would not be a freak occurrence to assume that their performance is heavily dependent on these HP settings. However, our closer analysis of the experiment testbeds in recent literature on deep OD models falls far from systematically addressing the issue. (See Appx. A.1 Table 6 for a preview.) We find hardly any discussion on model selection, with only a few work empirically studying sensitivity but to model-specific HPs only. Majority of work report results for a single “recommended” (how, unclear) configuration used for all datasets, or tune only a subset of the HPs on labeled validation and sometimes even test (!) data. To the best of our knowledge, there is no existing work that attempts (unsupervised) model selection for deep OD models.

In this work, our research goals are two-fold. **First**, through extensive experiments, we quantitatively demonstrate that deep OD models from various families are all sensitive to their HP settings. Our analysis shows that model selection is inevitable and is key to truly unlock the utmost potential of deep OD models. **Second**, motivated by our analysis, we propose a scalable deep *hyper-ensemble* called ROBOD that obviates HP selection through assembly of deep autoencoders with varying HP configurations. To speed up ensemble training, we introduce novel architectural and training strategies, and train fewer models, with fewer parameters, on smaller subsamples of data; by leveraging parameter sharing and joint/simultaneous training. The main contributions of our work are as follows.

- **First large-scale study on HP sensitivity of deep OD models:** We build a large testbed to systematically measure the performance variability of deep OD models under varying HP settings. Our study involves models from four different families, on both image and vector data, under both “clean” (i.e. inlier only) as well as “polluted” (i.e. outlier-contaminated) training data, over 3 random initializations, 80-800+ different HP configurations per model across 4-8 unique HPs. Overall, our analysis involves more than 35,000 runs. (Sec. 3)
- **ROBOD, a new deep hyper-ensemble OD model:** Motivated by our empirical study, we propose a hyper-ensemble model called ROBOD which combines scores from a collection of models, each trained with a different HP configuration. Rather than trying to choose, ROBOD fully bypasses the choice of and hence sensitivity to HP settings, and achieves robust (i.e. stable) performance across different initializations. (Sec. 4.1)
- **Design strategies to speed up hyper-ensemble training:** We propose speed-up strategies to efficiently hyper-ensemble model depth and width. We use an autoencoder (AE) with skip-connections to simultaneously train multiple AEs with different depths. In addition, we employ batch training of multiple models and use zero-masking on shared parameters to get different widths. Together, these provide a 90-98% savings in running time. (Sec. 4.2)
- **Extensive experiments:** Besides our large-scale measurement study, we also perform experiments on additional benchmark datasets, comparing ROBOD to baseline deep OD models as well as a traditional tree-ensemble. ROBOD achieves competitive or often better performance which, importantly, exhibits low variance by random initialization. (Sec. 5)

We expect that our work will increase awareness and help shift the community’s focus (at least to some extent) from building the next yet-another deep OD model toward the fundamental issue of unsupervised model selection and hyperparameter-robust model design. To foster future research, we open source all code and datasets at <https://anonymous.4open.science/r/9BD1-ROBOD>.

2 Related Work

Unsupervised Outlier Detection (OD). There exists a large pool of what-is-now-called traditional, i.e. not deep learning based, OD methods [10, 1]. These methods work with the original features or subspaces thereof, and typically exhibit just one or two hyperparameters (HPs).¹ With recent advances in deep learning, there has been a boom in deep OD models, as those can learn new task-dependent feature representations and directly optimize an OD objective. Despite their short history, multiple

¹e.g., k in nearest neighbor based LOF [7], ν in OCSVM [37], sample size ψ and #trees t in IF [27].

surveys have been published that aim to cover this fast-growing literature [30, 34, 9]. While deep OD models have been shown to outperform their traditional counterparts, they exhibit a much longer list of (typically 4-8) HPs (e.g. depth, width, dropout, weight decay, learning rate, epochs, etc. besides other model-specific HPs) that makes them very challenging to tune in unsupervised settings.

Model Selection in Unsupervised OD: Prior (Black) Art. At large, unsupervised outlier model selection remains to be a vastly understudied, yet extremely important area. Various evaluation studies have reported traditional detectors to be quite sensitive to their HP choices [2, 17, 8], raising concern for the fair evaluation and comparison of different models. Earlier work on automatically selecting HPs are limited to one-class models [38, 14, 39]. More recently, general-purpose *internal* (i.e., unsupervised) model evaluation heuristics have been proposed [28, 15, 29], which solely rely on the input data (without labels) and the output (i.e., outlier scores). MetaOD [44] employs meta-learning to transfer information from similar historical tasks to a new task for model selection, which has only been tested on traditional OD models. Different from those that aim to select a single model, ensemble models have also been employed for OD [3], including those that combine models from the same family [26] as well as heterogeneous detectors from different families [31].

Regarding deep OD methods, we have surveyed a large collection of recent papers and their experimental testbed and HP settings, a summary of which is given in Appx. A.1 Table 6. To our surprise, we found *hardly any discussion on model selection*, with only a few work presenting sensitivity analysis with respect to not all but some, model-specific HPs. While some work reserve labeled validation/hold-out data to tune a subset of the HPs [18, 23, 6], majority of them fix the HP values and call them “recommended”/default settings [11, 46, 35, 36, 43, 5]. Moreover, a non-negligible number of existing work choose some critical HPs empirically on test data (!) to yield optimum results [45, 33, 4] (See Table 6, last column). Some work that builds on previous models (e.g., deep SVDD-based methods [33] vs. multi-sphere extension [13], transformation-based methods [16] for images vs. their extension to vector data [5], AnoGAN [35] and the follow-up EGBAD [43]) use the same architecture and HP settings as the prior work for consistent/“fair” comparison. However it is unlikely that the same HP values would work comparably for different models.

Admittedly, it is challenging to tune (a long list of) HPs in the absence of labels, yet, the opacity in the deep OD literature warrants careful investigation on the stability of model performance under varying HP settings, and ultimately on the fair comparison between these and traditional OD methods.

Deep Model Ensembles. Recently, deep NN predictions have been found to be often poorly calibrated [20]. As Bayesian learning does not offer straightforward training, deep ensemble models have been proposed as a simple alternative [25] to improve predictive uncertainty, as well as efficient ways of training deep NN ensembles [40, 19]. In this work, we leverage ensemble modeling toward a different goal: to improve the stability and robustness of unsupervised OD models to HP settings, combining predictions from models with different HPs into an OD *hyper*-ensemble. The closest to our work is Wenzel *et al.*’s deep hyper-ensemble [41], which, different from ours, considers *supervised* problems, to further foster diversity in the ensemble and thereby achieve better uncertainty estimation.

3 Hyperparameter-Sensitivity Analysis of Deep OD

3.1 Testbed Setup

Models. We study HP sensitivity of five deep OD methods of four different types: a basic deep autoencoder VanillaAE trained with reconstruction loss, *robust* deep autoencoder RDA [45], *one-class* classification based DeepSVDD [33], *adversarial* training based GANomaly [4], and an (AE) *ensemble* model RandNet [11]. These exhibit 4 to 8 HPs, as listed in Table 1. (See Appx. A.2 for descriptions.) (Note that RandNet is **not** a **hyper**-ensemble: members use the same HP configs except for NN sparsity.) We define a grid of 2-3 different values for each HP, including the author-recommended values when available (See details in Appx. Table 7), and train each deep OD method with all combinations; yielding 81-864 different models. (Note that 192 RandNet models each consists of an ensemble of 50 or 200 AEs.) We repeat each experiment 3 times with different initializations.

Train/Test settings. In their original papers, DeepSVDD and GANomaly are trained on what we refer to as Clean (inlier only) data, and tested on a disjoint test dataset. In contrast, RDA and RandNet consider the *transductive* setting where the train data is the same as the test data, containing inliers as well as outliers, which we refer to as Polluted. It is often understood to be more challenging than the Clean setting for unsupervised OD. For completeness, we evaluate these methods under both settings.

Table 1: Deep OD models used for studying hyperparameter sensitivity. We give the number (in parenthesis) and the list of HPs for each method, along with the total number of models trained for evaluation. (See Appx. A.2 for HP descriptions and Appx. Table 7 for list of grid values per HP.)

Method	List of hyperparameters (HPs)	#models
VanillaAE	(4) $n_layers \cdot layer_decay \cdot LR \cdot iter$	81
RDA [45]	(6) $\lambda \cdot n_layers \cdot layer_decay \cdot LR \cdot inner_iter \cdot iter$	324
DeepSVDD [33]	(8) $conv_dim \cdot fc_dim \cdot Relu_slope \cdot pretr_iter \cdot pretr_LR \cdot iter \cdot LR \cdot wght_dc$	864
GANomaly [4]	(6) $w_{adv} = 1 \cdot w_{con} \cdot w_{enc} \cdot z_dim \cdot LR \cdot iter$	162
RandNet [11]	(8) $n_layers \cdot layer_decay \cdot sample_r \cdot ens_size \cdot pretr_iter = 100 \cdot iter \cdot LR \cdot wght_dc = 0$	192

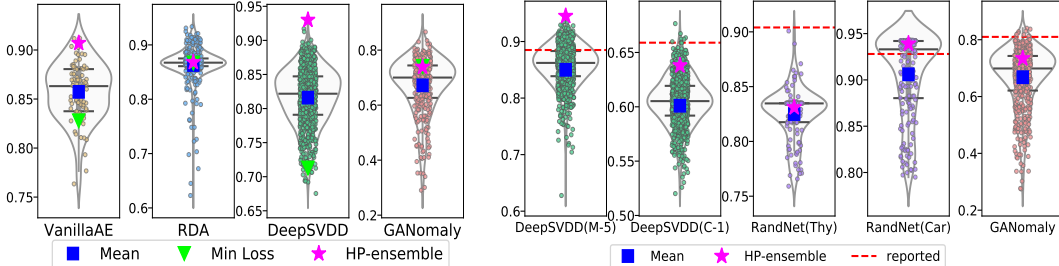


Figure 1: (left) AUROC performance of deep OD methods with different HP configurations (circles) on MNIST-4 showcase notable variation (i.e., sensitivity). (See footnote 2 below.) (right) Similar results on additional datasets; DeepSVDD on MNIST-5 and CIFAR10-auto, RandNet on Thyroid and Cardio, and GANomaly on MNIST-4-out. Reported values (dashed lines) are overestimates of Mean (□). Hyper-ensemble (☆) improves notably over Mean.

Datasets. For evaluation we consider both image point datasets. As in the original papers [33, 4], we use MNIST and CIFAR10 to construct OD tasks, except for RandNet which uses fully-connected rather than convolutional layers and is originally tested only on point-cloud benchmarks.

Metrics. Across all HP settings of a deep OD method, we report the mean AUROC, standard deviation (stdev), as well as minimum and maximum. Mean corresponds to the *expected* performance when a HP config is randomly picked from our (multi-dimensional) grid. We also report the average mean and its stdev over 3 repeated runs. For datasets that are directly comparable to those in the original papers, we contrast the mean model performance that we obtain to that reported value for author-recommended HPs. We compare to a simple model (i.e. HP) selection heuristic, which selects the (one) model with the lowest loss/objective value. In addition, instead of selecting one, we average the scores from *all* configurations and report the AUROC of this hyper-ensemble.

Over five deep OD methods, tens to hundreds of HP configs, multiple initializations, Clean and Polluted settings, and various datasets, we have trained a total of more than 35,000 models. As such, our study constitutes the first large-scale HP sensitivity analysis in the deep outlier mining literature.

3.2 Results and Observations

Fig. 1(left) provides the AUROC performances² for VanillaAE, RDA, DeepSVDD and GANomaly across all HP configurations (circles), for the Polluted setting (See Appx. A.3 Fig. 5 for Clean setting.) on MNIST-4 dataset where digit ‘4’ images are designated as inliers and the rest nine classes are down-sampled at 10% as outliers, as in the DeepSVDD paper [33]. Horizontal bars mark the 1st, 2nd (i.e. median), and 3rd quartiles, square the mean AUROC across HPs, triangle the selected model by lowest loss, and star the AUROC of the hyper-ensemble. (Corresponding plots over 3 runs per method are in Appx. A.3 Fig. 6.) Table 2 provides summary statistics as well as the hyper-ensemble performance for comparison for both the (left) Clean and (right) Polluted settings.

First, in Fig. 1 we observe that all methods exhibit notable variability in performance across HPs, with many worse-than-average configurations; e.g. for GANomaly, as well as many better-than-average models; e.g. for RDA. Mean performance is considerably lower than the best model’s, illustrating the opportunity or room for improvement. As one would expect, the performances in Table 2 are lower

²We remark that although the methods are presented side-by-side, the goal here is **not** to compare them “head-to-head” but rather, to analyze each one’s performance variability by varying HPs on individual datasets.

Table 2: Basic stats of AUROC (%) distribution over varying HPs on MNIST-4 under (left) Clean and (right) Polluted settings. There is significant gap between the best and worst HP settings, with notable stdev around the mean. Polluted results have lower mean, and comparable or slightly higher variance. Hyper-ensemble outperforms random choice (i.e. mean), with low variability by initialization.

Method	Min&Max	Mean&Std.	Mean (avg. 3 runs)	Hyper-ens. Mean (avg. 3 runs)	Min&Max	Mean&Std.	Mean (avg. 3 runs)	Hyper-ens. Mean (avg. 3 runs)
Vanilla AE	87.41	98.19	93.12 \pm 2.91	93.12 \pm 0.008	76.34	91.20	85.73 \pm 2.95	85.76 \pm 0.08
RDA	81.79	95.96	88.94 \pm 2.43	88.95 \pm 0.02	62.29	93.35	86.30 \pm 3.68	86.24 \pm 0.06
DeepSVDD	75.75	96.58	92.39 \pm 2.02	92.37 \pm 0.02	67.54	91.71	81.65 \pm 4.15	81.66 \pm 0.10
GANomaly	17.49	95.73	78.90 \pm 16.63	78.26 \pm 0.51	29.06	86.60	67.20 \pm 10.30	67.45 \pm 0.32

in the Polluted setting as compared to Clean (less so for the robust RDA), while sensitivity (i.e. stdev) is comparable or only slightly higher; showing that HP choice is critical under both settings.

We also find that selecting a model by the value of loss (∇), despite requiring to train and choose from all models, often is much worse than the mean, i.e. random picking a (single) model (\square); proving this simple heuristic ineffective. On the other hand, the hyper-ensemble (\star) outperforms the mean in all cases, with quite small standard deviation across runs (i.e. low sensitivity to initialization).

The reported performance (0.949 ± 0.008) of DeepSVDD on MNIST-4 (under Clean) [33] is similar yet somewhat optimistic over the mean value we obtain. MNIST-4 is an easy task for DeepSVDD since mean AUROC is already around 0.924. Thus, we set up MNIST-5 (with digit ‘5’ as inliers) with reported AUROC 0.885 ± 0.009 , as well as CIFAR10-auto (with class ‘automobile’ as inliers) (in both cases rest of the classes are subsampled at 10% each as outliers) with reported AUROC 0.659 ± 0.021 . We run DeepSVDD on both datasets under all 864 configurations. As shown in Fig. 1 (right), our mean AUROCs are 0.857 ± 0.037 for MNIST-5, and 0.605 ± 0.024 for CIFAR10-auto. (See Appx. A.3 Fig. 7 for all 3 runs.) The reported performances for the “recommended” HPs³ in DeepSVDD (dashed red lines) appear to be optimistic over the mean, i.e. what one would expect by random choice (in the absence of any labels or other strategies).

The optimistic reporting trend holds for GANomaly and RandNet as well. Following their original paper [4], and different from [33], we set up MNIST-4out dataset to contain digit ‘4’ images this time as the outliers and the rest nine classes as inliers. GANomaly performances across 162 HP configs are shown in Fig. 1 (right), where the reported result (red line) in [4] of AUROC 0.795 appears notably higher than the mean 0.668 ± 0.105 that we obtain. (See Appx. A.3 Fig. 8 for all 3 runs.)

For RandNet, we first find and verify a third-party implementation, as the authors could not publicly share theirs, by replicating similar performances to those reported in [11] using the author-recommended HP settings on all 8 datasets. Then for Cardio and Thyroid datasets, we train 192 RandNet ensembles with varying HPs under Polluted as in the original paper. Results from one run are shown in Fig. 1 (right). (See Appx. A.3 Fig. 9 for all 3 runs.) On Cardio, AUROC mean is 0.894 ± 0.045 vs. 0.929 (reported), and Thyroid mean is 0.822 ± 0.026 vs. 0.904 (reported).

In summary, the take-aways from our analysis are as follows. First, it is clear that deep OD models are sensitive to their HP settings, showing that model/HP selection is inevitable. The mean/expected value (of random choice) can be quite away from the best model, motivating this line of research. Second, the recommended settings in recent deep OD papers are arguably optimistic; otherwise more transparency into their selection mechanism is warranted. Finally, hyper-ensemble performance is superior to the mean, possibly owing to different HPs implicitly imposing diversity among constituent models which helps improve detection. Besides performance improvement, hyper-ensembling obviates model selection by joining all models rather than choosing one and is not much sensitive to initialization – setting the stage for our proposed HP-robust OD method ROBOD.

4 ROBOD: A Deep Hyper-ensemble for Hyperparameter-Robust OD

4.1 Motivation and Overview

The main research question we consider is **RQ1) how to design an unsupervised deep OD model that is robust to its HPs**, i.e. an OD method that has stable, low-variance predictions under varying HPs. Motivated by our sensitivity analysis in Sec. 3, we propose a deep autoencoder (AE) hyper-ensemble model that combines scores from AE models with different HP configurations.

³Besides fixed values for various HPs, Ruff *et al.* [33] recommend HPs that *differ by dataset*; e.g. on MNIST they use 2 CNN modules w/ size 8 and 4 filters, on CIFAR10 they use 3 modules w/ size 32, 64, and 128 filters.

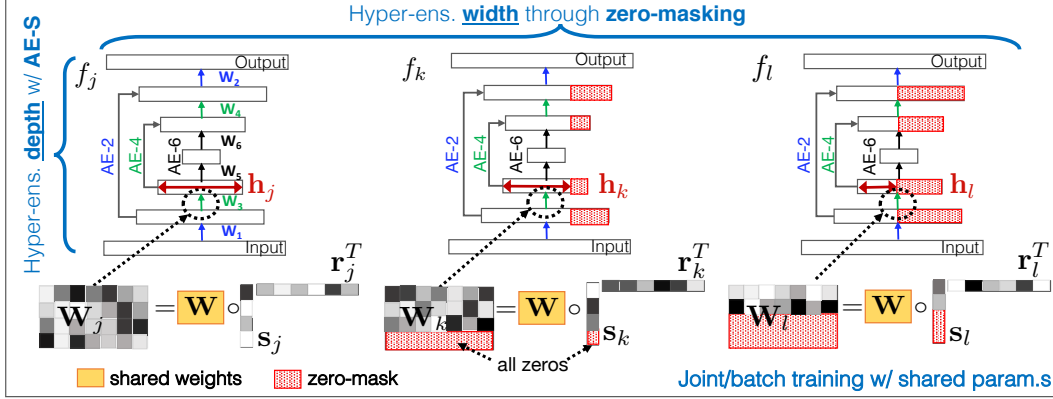


Figure 2: Main design elements in ROBOD: (1) **AE with Skip links (AE-S)**: Each AE-S, denoted f , hyper-ensembles multiple AE models with various depths (in the figure, AE-2, 4 and 6), with *shared parameters*; e.g. for f_j , layer 2 weights W_j (in dashed circle) is shared among different-depth AEs (i.e. AE-4 and AE-6). (2) **Batch ensemble (BE) training with zero-masks**: Multiple AE-S models with *shared parameters* are trained simultaneously, having various widths thanks to zero-masking; e.g. at layer 2, W is shared by all three different-width AE-S models in the batch (denoted f_j , f_k , f_l), where hidden sizes follow $|\mathbf{h}_j| > |\mathbf{h}_k| > |\mathbf{h}_l|$ through varying size zero-masks on s_k and s_l . (sr^T depicts an outer product, and \circ denotes Hadamard/element-wise matrix multiplication.)

Definition 1 (Hyper-ensemble) Given a model family \mathcal{M} with H HPs, let $\lambda \in \mathbb{R}^H$ denote a specific setting of the HPs. A hyper-ensemble averages the output (outlier scores) from a finite number of base models with m different config.s, i.e. $\frac{1}{m} \sum_{i=1}^m \mathcal{M}(\mathbf{x}; \lambda_i)$ for point \mathbf{x} .

Hyper-ensembles exhibit multiple advantages. First, and to our end goal, they ease the model/HP selection burden, bypassing the “choice paralysis”. They are less sensitive to random initializations, with lower variance in performance. Moreover, they can even boost detection performance thanks to the diversity offered by different HPs and ensemble prediction.

The caveat is that deep ensembles are computationally expensive to train. As such, the second research task we tackle is **RQ2) how to speed up hyper-ensemble training**. To that end, we propose novel architectural and training strategies. In a nutshell, these strategies involve three main ideas: (1) we design a multi-layer AE architecture with *skip* connections, denoted AE-S, that helps hyper-ensemble, under a *single* model, *varying-depth* AEs with *shared* parameters; (2) we employ batch ensemble training [40] of multiple AE-S models using *varying size zero-masking* that helps hyper-ensemble *varying-width* AEs all trained *simultaneously* with *shared* parameters; and (3) we train each AE-S on a *subsample* and use out-of-sample scoring. In effect, these strategies allow us to build fewer models, with fewer total number of parameters, on less training data—taking only 2-10% of the time that the naïve ensemble training would take where each model is trained independently.

Fig. 2 illustrates the main design elements of ROBOD pictorially. We present details of the architecture and the training as follows.

4.2 Design Strategies for Speeding up Ensemble Training

4.2.1 Hyper-ensembling depth: One model for multiple depths

Skip or shortcut connections are applied in NNs for various purposes; e.g., in ResNet [21] for solving the depth degradation problem, in JK-Net [42] for representation learning with varying localities, in U-Net [32] and stochastic depth NNs [24] for training models with adaptive depth, and so on.

Due to the “hourglass” structure of the AE, skipping one layer in an AE would cause dimensionality mismatch for the next layer. Instead, we create long shortcuts by skipping the middle layers while keeping the outer encoder-decoder pairs symmetrically, and refer to this architecture as AE-S.

An illustration of hyper-ensembling depth can be found in Fig. 2; see e.g. the AE-S denoted by f_j . Given a $2L$ -layer AE-S (L encoder and L decoder layers), there are $2L$ trainable weight matrices. For input \mathcal{D} , we generate L outputs by allowing the input to pass through the outermost encoder-decoder pair (which we denote as *AE-2*), the two outermost encoder-decoder pairs (*AE-4*), and so on, until the full structure (*AE-2L*) is traversed by the input. In effect, this trains L different AEs under *one*

AE-S model. Then, the overall loss \mathcal{L}_{AE-S} of the depth-hyper-ensembling AE-S is the summation of the member AEs' reconstruction errors (denoted ΔErr). Eq. (1) gives an example of the loss function for a 6-layer AE-S as shown in Fig. 2,

$$\mathcal{L}_{AE-S} = \Delta Err_{AE-2}(\mathcal{D}; [\mathbf{W}_1:\mathbf{W}_2]) + \Delta Err_{AE-4}(\mathcal{D}; [\mathbf{W}_1:\mathbf{W}_4]) + \Delta Err_{AE-6}(\mathcal{D}; [\mathbf{W}_1:\mathbf{W}_6]) \quad (1)$$

AE-S is an implicit hyper-ensemble which allows simultaneous/joint training of AEs with various depths. It is computationally efficient thanks to parameter sharing, as the outer layers' weights are reused and tuned among different members. Each ensemble member can also play a regularization effect and prevent an AE from producing low scores for outliers due to overfitting. (See Appx. A.4).

4.2.2 Hyper-ensembling width: Zero-masked joint training

BatchEnsemble [40] (BE) is a state-of-the-art parameter-efficient deep ensemble training approach. However, off-the-shelf, it does not allow for *hyper*-ensembling, that is, all models in the batch are trained with the same HP configuration, and share equal size parameters. Our approach builds on BE, adapting it to simultaneously train varying-width AE-S with shared parameters.

First, we briefly review the BE architecture with K AEs. For a specific layer in BE, weight $\mathbf{W} \in \mathbb{R}^{m \times r}$ is shared across all K individual members, while each member i maintains two trainable rank-1 vectors: $\mathbf{s}_i \in \mathbb{R}^m$ and $\mathbf{r}_i \in \mathbb{R}^r$. The outer product (\cdot) of \mathbf{r}_i and \mathbf{s}_i^T creates a “mask” (a matrix in $\mathbb{R}^{m \times r}$) onto the shared weight \mathbf{W} and generates individual weight $\overline{\mathbf{W}}_i$. For the input mini-batch $\mathbf{X}_i \in \mathbb{R}^{n \times m}$, the forward propagation computation is

$$\Phi(\mathbf{X}_i \overline{\mathbf{W}}_i) = \Phi(\mathbf{X}_i (\mathbf{W} \circ (\mathbf{s}_i \cdot \mathbf{r}_i^T))) = \Phi((\mathbf{X}_i \circ \mathbf{s}_i) \mathbf{W} \circ \mathbf{r}_i), \quad (2)$$

where Φ is the activation function, \circ is the element-wise product, and \mathbf{r}_i and \mathbf{s}_i are broadcasted row-wise or column-wise depending on the shapes at play. To vectorize the calculation for all K members in the ensemble, two matrices $\mathbf{S} \in \mathbb{R}^{K \times m}$ and $\mathbf{R} \in \mathbb{R}^{K \times r}$ are constructed with rows of \mathbf{s}_i and \mathbf{r}_i , respectively. Thus, for the input $\mathbf{X} \in \mathbb{R}^{Km \times n}$, the BE layer computes the next layer as

$$\Phi((\mathbf{X} \circ \mathbf{S}) \mathbf{W} \circ \mathbf{R}). \quad (3)$$

Since \mathbf{X} is composed of K mini-batching \mathbf{X}_i 's tiling up, each member can utilize a different mini-batch of input. The K members are training simultaneously in parallel using one forward pass, thus relieving the memory and computational burden of traditional ensemble methods.

While BE itself is not a hyper-ensemble, we can leverage this architecture to aggregate networks of different widths, also in an efficient way. The widths of a neural network layer correspond to the rows in the weight matrix. For a specific layer, instead of directly operating on \mathbf{W} , we instead initialize a zero-one masking vector $\alpha_i \in \{0, 1\}^r$. α_i is to element-wise multiply with the $\mathbf{r}_i \in \mathbb{R}^r$, such that the operation $\mathbf{W} \circ \mathbf{s}_i \cdot (\mathbf{r}_i^T \circ \alpha_i^T)$ will create a masking matrix of size $(m \times r)$ and sparsify the individual weight $\overline{\mathbf{W}}_i$ by allowing zero'ed-out rows. In vectorized notation, the matrix $\mathbf{A} \in \{0, 1\}^{K \times r}$ is composed of K distinct masking vectors. Then, the zero-masked BE forward propagation becomes

$$\Phi(\mathbf{X} \circ \mathbf{S}) \mathbf{W} \circ (\mathbf{R} \circ \mathbf{A}). \quad (4)$$

Sparsifying neural networks has been shown to decrease storage and improve training efficiency, with many algorithms built to wisely prune the neural network [22]. While zero-masked BE is similar to creating neural networks of varying density, our main goal is to obtain models with different widths (i.e. hidden sizes), such that when trained under BE, creates a width-hyper-ensemble. Specifically, we construct the zero-masked BE layer with the maximum width and specify the zeros in respective α vectors, such that the masked-out individual weights correspond to varying-width models.

The zero-masked BE is efficient as \mathbf{A} is fixed throughout training. The element-wise product of the masking incurs little extra time during forward and backward propagation, while all the (rank-1) vectors are cheap to store compared to separate weight matrices as in traditional ensemble training.

4.2.3 ROBOD: The overall hyper-ensemble

Let H denote the total number of HPs for an AE-S, where we define a grid of values for each HP; e.g. $\text{depth} = [4, 6, 8]$, $\text{width} = [64, 128, 256]$, $\text{lrn_rate} = [1e^{-3}, 5e^{-4}]$, $\text{drop_out} = [0.0, 0.2]$, etc.

For the two HPs, depth and width , we specify the AE-S with the largest depth value (following Sec. 4.2.1, say $2L$) in the grid and leverage the skip connections to obtain the smaller-depth AEs.

Similarly, we specify each AE-S in the zero-masked BE with the largest width value (following Sec. 4.2.2, say K) in the grid and leverage the zero-masking to obtain other, smaller-width AEs.

Then, a zero-masked BE trains in parallel K varying-width AE-S models, each being an ensemble of L varying-depth AEs. Outlier score for a point \mathbf{x} is averaged across all KL AE models as

$$s(\mathbf{x}) = \frac{1}{KL} \sum_{i=1}^K s_i(\mathbf{x}), \quad \text{where } s_i(\mathbf{x}) = \sum_{d=1}^L \|\mathbf{x} - f_i^{(AE-2d)}(\mathbf{x}; \boldsymbol{\lambda})\|^2, \quad (5)$$

where f_i is the i 'th AE-S member, $f_i^{(AE-2d)}$ denotes the AE associated with depth $2d$ within f_i , and $\boldsymbol{\lambda}$ is a vector depicting a specific configuration of all the remaining $(H-2)$ HPs; e.g. [$\text{lrn_rate} = 1e^{-3}$, $\text{drop_out} = 0.2$, etc.]. Denoting the total number such configurations by B , ROBOD averages scores, i.e. the $s(\mathbf{x})$ values, from B different zero-masked BEs as the final outlier score of \mathbf{x} .

4.2.4 Further speed up by subsampling

As shown in Eq. 2, BE allows mini-batching, where each data point can be used by one or several different ensemble members. This makes BE a natural fit to subsampling, which further expedites the training procedure. To this end, we create $\{\mathbf{X}_i^{in}, \mathbf{X}_i^{out}\}_{i=1}^K$ splits of the training data, where for each AE-S member i , we divide the training data into \mathbf{X}_i^{in} and $\mathbf{X}_i^{out} = \mathbf{X}_i / \mathbf{X}_i^{in}$ and solely train on mini-batches from \mathbf{X}_i^{in} . We then compute the out-of-sample⁴ outlier score of point \mathbf{x} as $s(\mathbf{x}) = \frac{1}{K'L} \sum_{i=1}^K \mathbb{1}(\mathbf{x} \in \mathbf{X}_i^{out}) s_i(\mathbf{x})$, where $K' = \sum_{i=1}^K \mathbb{1}(\mathbf{x} \in \mathbf{X}_i^{out})$.

5 Experiments

We conduct experiments to answer the following: **Q1.** How does ROBOD compare to state-of-the-art (SOTA) OD methods? **Q2.** How much does ROBOD's performance vary by initialization? **Q3.** What are the savings in running time compared to /naïve hyper-ensemble w/ independent training?

Baselines. We compare to SOTA *deep* OD methods VanillaAE, RDA [45], DeepSVDD [33] and RandNet [11], the latter of which is a deep AE ensemble. We also include the tree-ensemble Isolation Forest [27] (IF) which stands as the SOTA among *traditional* detectors [12]. Besides ROBOD without subsampling, we experiment with two subsampling versions, denoted ROBOD- δ , for sampling rates $\delta \in \{0.1, 0.5\}$. We also compare to the naïve ROBOD with independent training, denoted i-ROBOD.

Configurations. The baselines exhibit 2-8 HPs, per which we define a small grid of values (See Appx. A.5 Table 8). We report the expected AUROC performance, i.e., averaged across all configurations in the grid, along with the standard deviation. For ROBOD (and variants) we set $L=6$, and $K=8$; the other HP config.s are listed in Appx. Table 9. To measure sensitivity to random initialization, we average performance across 3 runs. All models are trained on a NVIDIA RTX A6000 GPUs server.

Datasets. We conduct experiments on 5 image datasets from MNIST and CIFAR10, as well as 3 tabular datasets from the ODDS repository.⁵ MNIST and CIFAR10 are multi-class, where we pick one class as the inliers and subsample the rest at 10% each to constitute outliers. Datasets have varying outlier % and size, with images having high dimensionality. (See Table 3; MNIST-4, -5, -8 depict respective digits as inliers. CIFAR10-0 and -1 refer to airplane and auto class as inliers, respectively.) Details on dataset description and preparation can be found in Appx. A.5.2. The experiments are all conducted under the Polluted (i.e., transductive) setting.

Table 3: Dataset statistics.

Name	# pts.	dim.	outl.%
MNIST-4	6426	$1 \times 28 \times 28$	10.0
MNIST-5	6426	$1 \times 28 \times 28$	10.0
MNIST-8	6426	$1 \times 28 \times 28$	10.0
CIFAR10-0	5500	$3 \times 32 \times 32$	10.0
CIFAR10-1	5500	$3 \times 32 \times 32$	10.0
Thyroid	3772		2.5
Cardio	1831		9.6
Lympho	148		4.1

Results. The main results are as shown in Table 4. **Q1.** ROBOD achieves superior performance to all deep OD baselines on MNIST and tabular datasets, and competitive performance on CIFAR10 datasets against the overall runner-up RandNet. Notably, ROBOD performs similarly or even better than i-ROBOD, the latter potentially owing to the guarding effect of parameter sharing against overfitting. Moreover, similar performance can be retained under subsampling, where we train each hyper-ensemble member with 50% or even 10% of the data.

⁴Applicable to transductive OD only; for inductive OD, a point is scored by all ensemble members.

⁵<http://odds.cs.stonybrook.edu/>

Table 4: AUROC (%) performance of OD methods. Baselines (top) avg.’ed across HP config.s, ROBOD and variants (bottom) avg.’ed over 3 runs w/ random init.s.; \pm one stdev. Entries in green depict the method w/ least variance. Highlighted in bold and underline are the **best** and runner-up.

	MNIST-4	MNIST-5	MNIST-8	CIFAR10-air	CIFAR10-auto	Cardio	Thyroid	Lympho
VanillaAE	81.4 \pm 9.4	73.6 \pm 10.1	83.3 \pm 4.6	60.3 \pm 2.0	59.2 \pm 4.7	87.1 \pm 7.7	81.1 \pm 8.5	89.4 \pm 11.7
RDA	79.7 \pm 11.2	68.9 \pm 11.4	82.6 \pm 10.2	53.9 \pm 8.8	54.1 \pm 8.9	78.4 \pm 12.1	80.9 \pm 5.3	78.0 \pm 12.2
DeepSVDD	81.9 \pm 4.3	75.7 \pm 3.8	85.3 \pm 3.9	55.6 \pm 3.1	59.0 \pm 3.0	54.6 \pm 7.9	67.5 \pm 15.1	66.5 \pm 15.6
RandNet	85.3 \pm 3.1	79.3 \pm 3.8	85.4 \pm 2.2	59.1 \pm 2.6	59.5 \pm 3.8	89.2 \pm 5.3	81.5 \pm 5.8	92.3 \pm 8.1
IF	84.2 \pm 0.8	70.5 \pm 1.5	42.9 \pm 0.5	62.7\pm0.8	94.1\pm0.9	97.9\pm0.4	99.5\pm0.3	
ROBOD	88.0\pm0.0	81.4\pm0.1	87.8 \pm 0.0	59.4 \pm 0.0	59.2 \pm 0.1	93.5\pm0.1	86.1 \pm 0.6	98.7 \pm 0.1
ROBOD-0.5	<u>86.7\pm0.1</u>	<u>78.5\pm0.1</u>	<u>88.1\pm0.1</u>	<u>59.6\pm0.5</u>	<u>58.4\pm0.3</u>	<u>92.1\pm0.3</u>	<u>87.9\pm1.3</u>	<u>98.7\pm0.1</u>
ROBOD-0.1	<u>86.7\pm0.0</u>	<u>78.5\pm0.1</u>	88.2\pm0.1	<u>59.3\pm0.0</u>	<u>58.3\pm0.2</u>	<u>91.8\pm0.3</u>	<u>88.4\pm0.5</u>	<u>99.0\pm0.1</u>
i-ROBOD	84.5 \pm 0.0	74.6 \pm 0.1	87.0 \pm 0.0	62.5\pm0.0	61.7 \pm 0.1	87.1 \pm 0.1	<u>93.0\pm0.0</u>	98.9 \pm 0.0

Q2. Importantly, the standard deviation (stdev) of the deep OD baselines is notably large, which is slightly smaller for the ensemble model RandNet, whereas ROBOD has significantly smaller stdev, with near-zero sensitivity to random initialization. The sensitivity of deep baselines suggests that in practice, with an arbitrary choice of HPs in the absence of any other guidance, one may acquire much less satisfactory outcomes than the average AUROC.

An interesting observation is regarding the traditional IF baseline, which excels on (low-dim.) tabular datasets, and remains competitive on MNIST-4 and CIFAR10-auto. It also shows relatively small variance w.r.t. its (two) HPs. However, it is significantly inferior on other high-dim. image OD tasks, which may be attributed to its lack of representation learning. Nevertheless, the competitiveness of this simple baseline suggests that traditional OD methods cannot be ignored in the ‘horse-race’ of developing new deep OD methods, not only for their competitiveness but also for their robustness to only-a-few HPs that makes them easy to employ by practitioners.

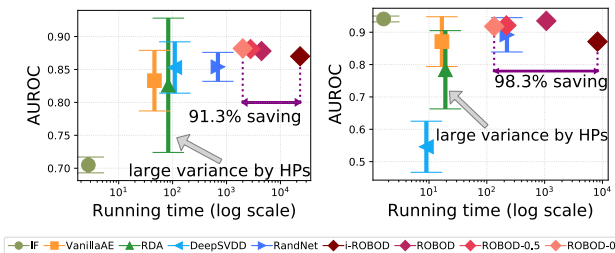


Figure 3: Running time (in log scale) vs. AUROC performance of OD methods (symbols) on (left) MNIST-8 and (right) Cardio. Vertical bars depict one (1) stdev across HP config.s for the baselines.

In Fig. 3 we show the running time (in sec.s) versus the performance for all OD methods (colored symbols) on one image and one tabular dataset for brevity. (See Appx. A.6 Fig. 11 for remaining datasets.) ROBOD achieves higher performance, with lower, near-zero variability compared to deep baselines. Traditional IF, based on randomized trees, is very fast, yet it often underperforms on high dimensional tasks such as with images.

Q3. Finally, we study the savings that ROBOD offers compared to the naïve hyper-ensembling. As shown in Table 5, it runs 3-10 \times faster across datasets. With subsampling at 10%, ROBOD-0.1 runs in about 1.6-10% of what it takes by i-ROBOD. Fig. 4, based on MNIST-5, shows that while i-ROBOD time increases by the number of models, i.e. larger L and K (having other HPs fixed), ROBOD takes near-constant time thanks to the batch/simultaneous training of varying-depth and varying-width members.

Table 5: Running time (sec.) of the naïve ensemble i-ROBOD vs. ROBOD. ROBOD-0.1 that trains with 10% subsampling offers 90-98% relative savings in training time.

	MT-4	MT-5	MT-8	CIF-air	CIF-auto	Cardio	Thy.	Lym.
i-ROBOD	24192	24656	23165	38830	39562	8205	14313	1804
ROBOD	4521	4630	4456	10721	10722	1070	2049	180
ROBOD-0.1	2241	2141	1997	2834	3003	134	295	44

Savings (%) 90.74 91.32 91.38 92.70 92.41 98.37 97.94 97.56

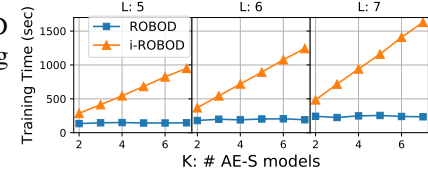


Figure 4: Runtime comparison of ROBOD to i-ROBOD w/ varying L and K .

6 Conclusion

In this work, we have provided a thorough analysis on the hyperparameter (HP) sensitivity of several state-of-the-art deep outlier detection (OD) methods. Our findings quantitatively confirm that model selection is vital and advocate efforts in this line of research. To this end, we introduce ROBOD,

a scalable hyper-ensemble OD method that remedies the “choice paralysis” by assembling various autoencoder models of different HP configurations, hence obviating HP/model selection. We speed up ensemble training through novel strategies that simultaneously train varying depth and width models under parameter sharing. Extensive experiments on image and point-cloud datasets show the competitiveness of ROBOD compared to existing OD baselines, while providing consistent results across random initializations. We hope that our work increases awareness to the unsupervised model selection challenge for the newly booming deep OD literature and motivates future work on hyperparameter-robust model design.

References

- [1] C. C. Aggarwal. *Outlier Analysis*. Springer Publishing Company, Incorporated, 2nd edition, 2016. ISBN 3319475770.
- [2] C. C. Aggarwal and S. Sathe. Theoretical foundations and algorithms for outlier ensembles. *SIGKDD Explor.*, 17(1):24–47, 2015.
- [3] C. C. Aggarwal and S. Sathe. *Outlier ensembles: An introduction*. Springer, 2017.
- [4] S. Akcay, A. Atapour-Abarghouei, and T. P. Breckon. Gandomaly: Semi-supervised anomaly detection via adversarial training. In *Asian conference on computer vision*, pages 622–637. Springer, 2018.
- [5] L. Bergman and Y. Hoshen. Classification-based anomaly detection for general data. In *ICLR*, 2020. URL https://openreview.net/forum?id=H11K_1BtvS.
- [6] A. Boyd, R. Bamler, S. Mandt, and P. Smyth. Neural transformation learning for deep anomaly detection beyond images. In *34th Conference on Neural Information Processing Systems*, 2020.
- [7] M. M. Breunig, H.-P. Kriegel, R. T. Ng, and J. Sander. LOF: Identifying density-based local outliers. In *SIGMOD Conference*, pages 93–104. ACM, 2000. URL <http://dblp.uni-trier.de/db/conf/sigmod/sigmod2000.html#BreunigKNS00>. SIGMOD Record 29(2), June 2000.
- [8] G. O. Campos, A. Zimek, J. Sander, R. J. G. B. Campello, B. Micenková, E. Schubert, I. Assent, and M. E. Houle. On the evaluation of unsupervised outlier detection: measures, datasets, and an empirical study. *Data Min. Knowl. Discov.*, 30(4):891–927, 2016. doi: 10.1007/s10618-015-0444-8. URL <https://doi.org/10.1007/s10618-015-0444-8>.
- [9] R. Chalapathy and S. Chawla. Deep learning for anomaly detection: A survey, 2019. URL <http://arxiv.org/abs/1901.03407>. cite arxiv:1901.03407.
- [10] V. Chandola, A. Banerjee, and V. Kumar. Anomaly detection: A survey. *ACM Computing Surveys*, 41(3):15:1–15:58, July 2009. ISSN 0360-0300. doi: 10.1145/1541880.1541882. URL <http://doi.acm.org/10.1145/1541880.1541882>.
- [11] J. Chen, S. Sathe, C. C. Aggarwal, and D. S. Turaga. Outlier detection with autoencoder ensembles. In N. V. Chawla and W. Wang, editors, *SDM*, pages 90–98. SIAM, 2017. ISBN 978-1-61197-497-3. URL <http://dblp.uni-trier.de/db/conf/sdm/sdm2017.html#ChenSAT17>.
- [12] A. Emmott, S. Das, T. Dietterich, A. Fern, and W.-K. Wong. A meta-analysis of the anomaly detection problem. *arXiv preprint arXiv:1503.01158*, 2015.
- [13] Z. Ghafoori and C. Leckie. Deep multi-sphere support vector data description. In *SDM*, pages 109–117. SIAM, 2020.
- [14] Z. Ghafoori, S. M. Erfani, S. Rajasegarar, J. C. Bezdek, S. Karunasekera, and C. Leckie. Efficient unsupervised parameter estimation for one-class support vector machines. *IEEE transactions on neural networks and learning systems*, 29(10):5057–5070, 2018.
- [15] N. Goix. How to evaluate the quality of unsupervised anomaly detection algorithms? *CoRR*, abs/1607.01152, 2016. URL <http://dblp.uni-trier.de/db/journals/corr/corr1607.html#Goix16>.

[16] I. Golan and R. El-Yaniv. Deep anomaly detection using geometric transformations. In S. Bengio, H. M. Wallach, H. Larochelle, K. Grauman, N. Cesa-Bianchi, and R. Garnett, editors, *NeurIPS*, pages 9781–9791, 2018. URL <http://dblp.uni-trier.de/db/conf/nips/nips2018.html#GolanE18>.

[17] M. Goldstein and S. Uchida. A comparative evaluation of unsupervised anomaly detection algorithms for multivariate data. *PLOS*, 11(4), 2016.

[18] S. Goyal, A. Raghunathan, M. Jain, H. V. Simhadri, and P. Jain. Drock: Deep robust one-class classification. In *International Conference on Machine Learning*, pages 3711–3721. PMLR, 2020.

[19] H. Guan, L. K. Mokadam, X. Shen, S.-H. Lim, and R. M. Patton. Fleet: Flexible efficient ensemble training for heterogeneous deep neural networks. In I. S. Dhillon, D. S. Papailiopoulos, and V. Sze, editors, *MLSys*. mlsys.org, 2020. URL <http://dblp.uni-trier.de/db/conf/mlsys/mlsys2020.html#GuanMSLP20>.

[20] C. Guo, G. Pleiss, Y. Sun, and K. Q. Weinberger. On calibration of modern neural networks. In *International Conference on Machine Learning*, pages 1321–1330, 2017.

[21] K. He, X. Zhang, S. Ren, and J. Sun. Deep residual learning for image recognition. In *CVPR*, pages 770–778. IEEE Computer Society, 2016. ISBN 978-1-4673-8851-1. URL <http://dblp.uni-trier.de/db/conf/cvpr/cvpr2016.html#HeZRS16>.

[22] T. Hoefler, D. Alistarh, T. Ben-Nun, N. Dryden, and A. Peste. Sparsity in deep learning: Pruning and growth for efficient inference and training in neural networks. *Journal of Machine Learning Research*, 22(241):1–124, 2021.

[23] W. Hu, M. Wang, Q. Qin, J. Ma, and B. Liu. Hrn: A holistic approach to one class learning. *Advances in Neural Information Processing Systems*, 33:19111–19124, 2020.

[24] G. Huang, Y. Sun, Z. Liu, D. Sedra, and K. Q. Weinberger. Deep networks with stochastic depth. In B. Leibe, J. Matas, N. Sebe, and M. Welling, editors, *ECCV (4)*, volume 9908 of *Lecture Notes in Computer Science*, pages 646–661. Springer, 2016. ISBN 978-3-319-46492-3. URL <http://dblp.uni-trier.de/db/conf/eccv/eccv2016-4.html#HuangSLSW16>.

[25] B. Lakshminarayanan, A. Pritzel, and C. Blundell. Simple and scalable predictive uncertainty estimation using deep ensembles. In I. Guyon, U. von Luxburg, S. Bengio, H. M. Wallach, R. Fergus, S. V. N. Vishwanathan, and R. Garnett, editors, *NIPS*, pages 6402–6413, 2017. URL <http://dblp.uni-trier.de/db/conf/nips/nips2017.html#Lakshminarayanan17>.

[26] A. Lazarevic and V. Kumar. Feature bagging for outlier detection. In R. Grossman, R. J. Bayardo, and K. P. Bennett, editors, *KDD*, pages 157–166. ACM, 2005. ISBN 1-59593-135-X. URL <http://dblp.uni-trier.de/db/conf/kdd/kdd2005.html#LazarevicK05>.

[27] F. T. Liu, K. M. Ting, and Z.-H. Zhou. Isolation forest. In *ICDM*, pages 413–422. IEEE Computer Society, 2008. ISBN 978-0-7695-3502-9. URL <http://dblp.uni-trier.de/db/conf/icdm/icdm2008.html#LiuTZ08>.

[28] H. O. Marques, R. J. G. B. Campello, A. Zimek, and J. Sander. On the internal evaluation of unsupervised outlier detection. In *SSDBM*, pages 7:1–7:12. ACM, 2015. URL <http://dblp.uni-trier.de/db/conf/ssdbm/ssdbm2015.html#MarquesCZS15>.

[29] V. Nguyen, T. Nguyen, and U. Nguyen. An evaluation method for unsupervised anomaly detection algorithms. *Journal of Computer Science and Cybernetics*, 32(3):259–272, 2017. ISSN 1813-9663. doi: 10.15625/1813-9663/32/3/8455. URL <http://vjs.ac.vn/index.php/jcc/article/view/8455>.

[30] G. Pang, C. Shen, L. Cao, and A. V. D. Hengel. Deep learning for anomaly detection: A review. *ACM Computing Surveys (CSUR)*, 54(2):1–38, 2021.

[31] S. Rayana and L. Akoglu. Less is more: Building selective anomaly ensembles. *ACM Trans. Knowl. Discov. Data*, 10(4):42:1–42:33, 2016. URL <http://dblp.uni-trier.de/db/journals/tkdd/tkdd10.html#RayanaA16>.

[32] O. Ronneberger, P. Fischer, and T. Brox. U-net: Convolutional networks for biomedical image segmentation. In N. Navab, J. Hornegger, W. M. Wells, and A. F. Frangi, editors, *Medical Image Computing and Computer-Assisted Intervention – MICCAI 2015*, pages 234–241, Cham, 2015. Springer International Publishing. ISBN 978-3-319-24574-4.

[33] L. Ruff, N. Görnitz, L. Deecke, S. A. Siddiqui, R. A. Vandermeulen, A. Binder, E. Müller, and M. Kloft. Deep one-class classification. In J. G. Dy and A. Krause, editors, *ICML*, volume 80, pages 4390–4399. PMLR, 2018. URL <http://proceedings.mlr.press/v80/ruff18a/ruff18a.pdf>.

[34] L. Ruff, J. R. Kauffmann, R. A. Vandermeulen, G. Montavon, W. Samek, M. Kloft, T. G. Dietterich, and K.-R. Müller. A unifying review of deep and shallow anomaly detection. *Proceedings of the IEEE*, 109(5):756–795, May 2021. ISSN 1558-2256. doi: 10.1109/JPROC.2021.3052449.

[35] T. Schlegl, P. Seeböck, S. M. Waldstein, U. Schmidt-Erfurth, and G. Langs. Unsupervised anomaly detection with generative adversarial networks to guide marker discovery. In M. Niethammer, M. Styner, S. R. Aylward, H. Zhu, I. Oguz, P.-T. Yap, and D. Shen, editors, *IPMI*, volume 10265 of *Lecture Notes in Computer Science*, pages 146–157. Springer, 2017. ISBN 978-3-319-59050-9. URL <http://dblp.uni-trier.de/db/conf/ipmi/ipmi2017.html#SchleglSWSL17>.

[36] T. Schlegl, P. Seeböck, S. M. Waldstein, G. Langs, and U. Schmidt-Erfurth. f-anogan: Fast unsupervised anomaly detection with generative adversarial networks. *Medical Image Anal.*, 54:30–44, 2019. URL <http://dblp.uni-trier.de/db/journals/mia/mia54.html#SchleglSWSL19>.

[37] B. Schölkopf, R. C. Williamson, A. J. Smola, J. Shawe-Taylor, and J. C. Platt. Support vector method for novelty detection. In *NIPS*, pages 582–588. The MIT Press, 1999. URL <http://dblp.uni-trier.de/db/conf/nips/nips1999.html#ScholkopfWSSP99>.

[38] D. M. Tax and R. P. Duin. Outliers and data descriptions. In *Proceedings of the 7th Annual Conference of the Advanced School for Computing and Imaging*, pages 234–241, 2001.

[39] S. Wang, Q. Liu, E. Zhu, F. Porikli, and J. Yin. Hyperparameter selection of one-class support vector machine by self-adaptive data shifting. *Pattern Recognition*, 74:198–211, 2018.

[40] Y. Wen, D. Tran, and J. Ba. BatchEnsemble: an alternative approach to efficient ensemble and lifelong learning. In *ICLR*. OpenReview.net, 2020. URL <http://dblp.uni-trier.de/db/conf/iclr/iclr2020.html#WenTB20>.

[41] F. Wenzel, J. Snoek, D. Tran, and R. Jenatton. Hyperparameter ensembles for robustness and uncertainty quantification. *arXiv preprint arXiv:2006.13570*, 2020.

[42] K. Xu, C. Li, Y. Tian, T. Sonobe, K.-i. Kawarabayashi, and S. Jegelka. Representation Learning on Graphs with Jumping Knowledge Networks. volume 80 of *Proceedings of Machine Learning Research*, pages 5453–5462, Stockholm, Sweden, 2018. PMLR. URL <http://proceedings.mlr.press/v80/xu18c.html>.

[43] H. Zenati, C. S. Foo, B. Lecouat, G. Manek, and V. R. Chandrasekhar. Efficient gan-based anomaly detection. *arXiv preprint arXiv:1802.06222*, 2018.

[44] Y. Zhao, R. Rossi, and L. Akoglu. Automatic unsupervised outlier model selection. In *Thirty-Fifth Conference on Neural Information Processing Systems*, 2021.

[45] C. Zhou and R. C. Paffenroth. Anomaly detection with robust deep autoencoders. In *KDD*, pages 665–674. ACM, 2017. ISBN 978-1-4503-4887-4. URL <http://dblp.uni-trier.de/db/conf/kdd/kdd2017.html#ZhouP17>.

[46] B. Zong, Q. Song, M. R. Min, W. Cheng, C. Lumezanu, D. ki Cho, and H. Chen. Deep autoencoding gaussian mixture model for unsupervised anomaly detection. In *ICLR*. OpenReview.net, 2018. URL <http://dblp.uni-trier.de/db/conf/iclr/iclr2018.html#ZongSMCLCC18>.

A Appendix

A.1 Preview of Existing Deep OD Methods

Table 6: Representative unsupervised deep OD models from 4 different families (for a broader coverage, see surveys [30, 34, 9]), annotated in terms of data used for training, test, and validation/model selection (if any). No existing work attempts (unsupervised) model selection; vast majority reports results for a *fixed* (how, unclear) “recommended” config. or tune *some* but not all HPs using labeled validation and even test (!) data. AE: autoencoder, SSL: self-supervised learning, Clean: inlier-only.

Method	Year	Family	Train	Test	Validation (HP/Model Selection)
RandNet [11]	2017	AE ensemble	Polluted	=Train	None, fixed – sensitivity analysis on some HPs
RDA [45]	2017	AE	Polluted	=Train	Best λ on Test, other HPs fixed
DAGMM [46]	2018	AE & density	Clean & Pol.d	Disjoint	None, fixed – sensitivity on reg. param.s $\{\lambda_1, \lambda_2\}$
DeepSVDD [33]	2018	One-Class	Clean	Disjoint	Best ν on Test, other HPs fixed
DROCC [18]	2020	One-Class	Clean	Disjoint	Validation data to tune some (not all) HPs
HRN [23]	2020	One-Class	Clean	Disjoint	10% of Test for tuning $\{\lambda, n\}$, other HPs fixed
(f-)AnoGAN [35, 36]	2017	GAN	Clean & Pol.d	Disjoint	None, fixed
EGBAD [43]	2018	(Bi)GAN	Clean	Disjoint	None, fixed
GANomaly [4]	2018	GAN	Clean	Disjoint	Best reg. weights $\{w_{adv}, w_{con}, w_{enc}\}$ on Test, others fixed
GOAD [5]	2020	SSL	Clean	Disjoint	None, fixed
NeuTraL [6]	2020	SSL	Clean	Disjoint	10% of Test for tuning transformation HPs, others fixed

A.2 Details on Hyperparameter-Sensitivity Analysis

Clean versus Polluted Testbed Setup. For sensitivity analysis, we construct our testbed on several datasets, including MNIST, CIFAR10, Thyroid and Cardio. For MNIST, we choose Digit ‘4’ and ‘5’ as the inlier-class, individually. For CIFAR10, we choose class ‘automobile’ as the inlier-class. The inlier-class is assigned the label 0, while we regard all classes other than the inlier-class as outliers and mark them with label 1 instead. Since MNIST and CIFAR10 are image data, we first apply the global contrast normalization to each individual image. We utilize the default train/test data-split (supported with Pytorch vision package). In the Clean setting, we select only the inlier-class data from train data-split as the training data. We measure and report the AUROC of the compared methods on the test data-split, with label 0 being the inlier-class and 1 being rest of the classes. In the Polluted setting, we utilize all the inlier-class data from the train data-split as the label 0, and we mix the data with 10% outlier-classes’ data within the train data-split.

The tabular data, Thyroid and Cardio, are downloaded from the ODDS repository (available at <http://odds.cs.stonybrook.edu/>). The data come in Polluted setting, with 2.5% and 9.6% outliers, respectively. The inliers are labeled 0 and outliers are denoted as label 1. For tabular data, we transform and scale each feature between zero and one.

We also conduct experiment using GANomaly [4]’s data (MNIST digit ‘4’ as the outlier class, rest as inliers). The data split and configuration are the same as described in the authors’ provided code.

Model HP Descriptions and Grid of Values.

- VanillaAE:
 1. `n_layers`: number of encoder layers (i.e. depth)
 2. `layer_decay`: the rate of NN width’s shrinkage between current and next encoder layers, the decoder layers are expanded at the same rate.
 3. `LR`: learning rate
 4. `iter`: number of epochs/iterations
- RDA:
 1. λ (model-specific reg.): a penalty term that tunes the level of sparsity in the outlier matrix S (refer to Section 3.1 in [45]).
 2. `n_layers`: number of encoder layers (i.e. depth)
 3. `layer_decay`: the rate of NN width’s shrinkage between current and next encoder layers, the decoder layers are expanded at the same rate.
 4. `LR`: learning rate
 5. `inner_iter`: number of epochs/iterations to train the underlying autoencoder (AE), before updating the outlier matrix S and inlier matrix L (refer to Section 4.1 in [45]).
 6. `iter`: number of epochs/iterations in the algorithm, which first separates the training data into outlier matrix S and inlier matrix L , then trains AE on the inlier matrix.

Table 7: We define a grid of 1-3 unique values for each hyperparameter (HP) of each deep OD method studied. With 4-to-8 different HPs each, the total number of configurations, and i.e. models trained, quickly grows to several hundreds. When applicable/available, we include the **author-recommended** value (marked in bold and underlined) in the respective grid.

Method	Hyperparameter	Grid	#values	Method	Hyperparameter	Grid	#values
VanillaAE	n_layers	[2, 3, 4]	3	DeepSVDD	conv_dim	[8 , 16, 32]	3
	layer_decay	[1, 2, 4]	3		fc_dim	[16 , 32]	2
	LR	[1e-3, 1e-4, 1e-5]	3		Relu_slope	[1e-1 , 1e-3]	2
	iter	[200, 500, 1000]	3		pretr_iter	[200, 350 , 400]	3
		Total =	81		pretr_LR	[1e-4, 1e-5]	2
RDA	λ	[5e-1, 5e-3, 5e-5]	3		iter	[100, 200, 250]	3
	n_layers	[2, 3, 4]	3		LR	[1e-4, 1e-5]	2
	layer_decay	[1, 2, 4]	3		wght_dc	[1e-5, 1e-6]	2
	LR	[1e-3, 1e-4]	2			Total #models =	864
	inner_iter	[20, 50]	2	RandNet	n_layers	[3, 5, 7 , 9]	4
GANomaly	iter	[5, 20, 50]	3		layer_decay	[0.3, 0.6]	2
	w_{adv}	1	1		sample_r	[1.00, 1.01]	2
	w_{con}	[25, 50 , 100]	3		ens_size	[50 , 200]	2
	w_{enc}	[0.1, 1]	2		pretr_iter	100	1
	z_{dim}	[50, 100 , 200]	3		iter	[300 , 1000]	2
GANomaly	LR	[5e-3, 2e-3 , 5e-4]	3		LR	[1e-2, 1e-3, 1e-4]	3
	iter	[10, 15 , 25]	3		wght_dc	0	1
			Total #models =				Total #models = 192
			162				

- DeepSVDD:
 1. conv_dim: the output number of channels, after the first- convolutional encoder layer. After the first-layer, the number of channels expand at rate of 2.
 2. fc_dim: the output dimension of the fully connected layer between convolutional encoder layers and decoder layers, in the LeNet structure [?].
 3. Relu_slope: DeepSVDD utilizes leaky-relu activation to avoid the trivial, uninformative solutions [33]. Here we alter the leakiness of the relu sloping.
 4. pretr_iter: In [33], an AE is pre-trained, to set the hypersphere center c to the mean of the mapped data. pretr_iter determines the number of epochs/iterations to train AE.
 5. pretr_LR: the learning rate to pretrain the AE.
 6. iter: the number of epochs/iterations in training the DeepSVDD
 7. LR: the learning rate during training
 8. wght_dc: weight decay rate
- GANomaly
 1. w_{adv} : weight parameter that adjusts the adversarial loss function (See Section 3.2 in [4].)
 2. w_{con} : weight parameter that adjusts the contextual loss, for learning the contextual information about the input data (See Section 3.2 in [4].)
 3. w_{enc} : weight parameter that adjusts the encoder loss and minimizes the distance between the bottleneck features and the encoder of the generated features (See Section 3.2 in [4].)
 4. z_{dim} : the dimension of the reduced embedded space after the input is passed through the encoders
 5. LR: learning rate
 6. iter: number of epochs/iterations
- RandNet
 1. n_layers: number of encoder layers (i.e. depth) in BAE
 2. layer_decay: the rate of NN width's shrinkage between current and next encoder layers, the decoder layers are expanded at the same rate.
 3. sample_r: sample size selection for adaptive sampling (See Section 3.3 in [3].)
 4. ens_size: number of ensemble members/models
 5. pretr_iter: number of epochs/iterations to pretrain the BAE
 6. iter: number of epochs/iterations
 7. LR: learning rate
 8. wght_dc: weight decay rate

A.3 Additional Results: Hyperparameter-Sensitivity Analysis

In Fig. 5, we show the AUROC performance of deep OD methods in Clean setting. In Fig. 6, Fig. 7, Fig. 8 and Fig. 9 we show additional experiment results and AUROC performances over 3 runs with different random initializations.

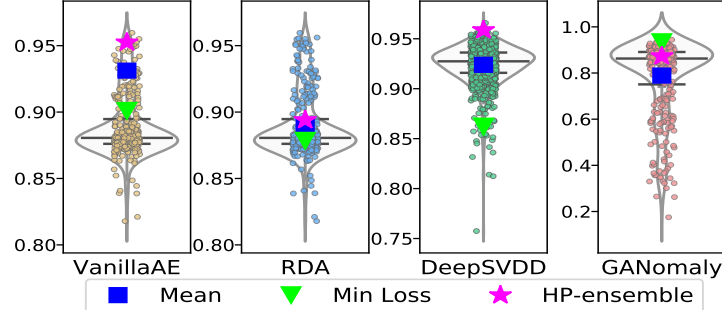


Figure 5: AUROC performance of deep OD methods with different HP configurations (circles) on MNIST-4 with Clean training data showcase notable variation (i.e., sensitivity). Hyper-ensemble (\star) improves notably over Mean (\square).

A.4 Regularization Effect of Weight Sharing

One noticeable problem with applying autoencoders (AE) and reconstruction loss for outlier detection is that for AE, the decision boundary is hard to draw due to noise and outliers that can impact the quality of the reconstruction. In some cases, the AE can overfit to all the data points including the outliers, causing large false negative rate. In other cases, it may underfit to data and fail to reconstruct the input satisfactorily. While the “denoising AEs” [?] or “correntropy AEs” [?] may help to alleviate such problems, they both rely on *clean* inlier-only data, which is typically not available in real-world scenarios. On the other hand, ROBOD with AE-S allows an implicit ensemble of various NN depths and widths and plays a regularization effect on the outliers scores, in effect helping prevent AE from potential failures due to underfitting or overfitting.

To demonstrate the regularization effect with AE-S, we compare the reconstructed images of AE versus AE-S, with number of layers $\{2, 4, 6, 8, 10, 12, 14\}$, respectively (hidden dimension decays at a constant rate of 2). We compare the individual AE and AE-S, keeping the other HP-configurations same, and training under the Polluted setting with MNIST digit ‘5’ as the inlier class. Fig. 10 shows the reconstructed images with these 7 individual AEs and a single AE-S ensemble, with implicit AE-i ($i \in \{2 \dots 14\}$). We see that individual AEs are overfitting to the outlier classes (digit ‘3’ and ‘7’) providing good reconstructions when layers L equal to 2 and 4. In contrast, they underfit and fail to reconstruct any inliers or outliers when layers L equals to 6, 8, and 10. When L increases to 12 and 14 layers, individual AEs provide low-quality reconstructions to both inliers and outliers, distorting all outliers to inlier class (digit ‘5’). In contrast, AE-S provides lower-resolution reconstruction for outlier classes during AE-2 and AE-4, that is overfitting showcases at a lower degree. AE-S can still provide signal to distinguish the outliers from the inliers from AE-6 through AE-12 where the outliers gradually become more blurred and start to deform into inlier’s shape. Only at very large depth at AE-14, AE-S cannot distinguish between outlier instances from inlier instances, providing low quality predictions to both classes.

Intuitively, this regularization effect is due to the weight sharing between AE-i’s. Since the next AE-i utilizes the weights optimized by the previous AE-i, the training phase becomes easier and underfitting is less likely to occur. Moreover, AE-S has a similar structure as U-Net [32], which is known to reduce the overfitting in medical image segmentation tasks.

While both i-ROBOD and ROBOD average the reconstruction loss from ensemble members, ROBOD with AE-S structure (and hence parameter sharing) is able to better capture the outlier information thanks to this regularization effect. This phenomenon also explains why ROBOD’s performance is better than that of i-ROBOD, e.g. on MNIST datasets in Table 4.

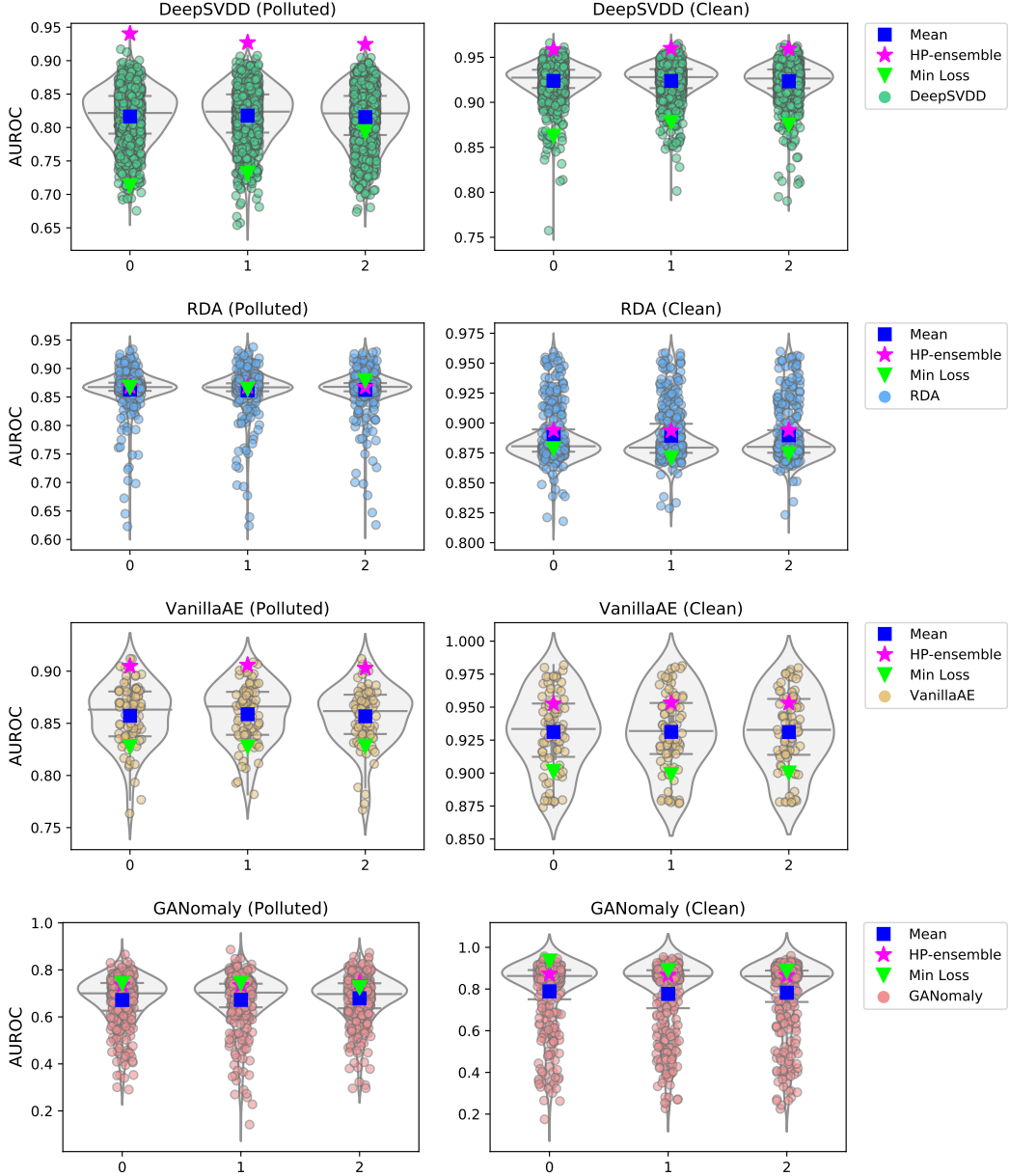


Figure 6: AUROC results under varying HP-configurations on MNIST-4 dataset under the Clean (only train on digit ‘4’ images) and Polluted (digit ‘4’ as inliers, the rest nine classes down-sampled at 10% as outliers) settings. We conduct each experiment 3 times with different random initialization, where each plot’s x-axis corresponds to the experiment index. Note: y-axes are not directly comparable – we use different y-axis to better reflect the spread for each experiment.

A.5 Details on Experiment Setup

A.5.1 Hyperparameter Configurations: Details

In experiments, we compare to VanillaAE, RDA [45], DeepSVDD [33] and RandNet [11]. We have not compared to GANomaly due to the higher variance of performances we observed during sensitivity analysis. We define a small grid of values for the HPs of each of these methods.

Because DeepSVDD is originally trained with LeNet [?] (Convolutional AE) structure, we also implement Convolutional AEs for algorithms that are either pretrained with AEs, or utilize AEs as the backbone algorithm. The detailed HP configurations are shown in Table 8. The VanillaAE and

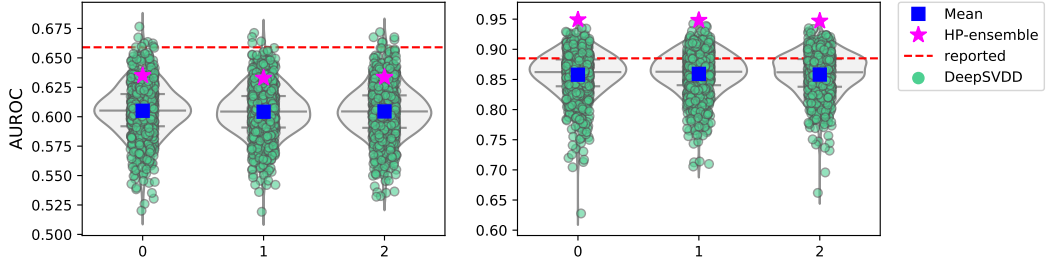


Figure 7: For DeepSVDD algorithm, we show various HP-configurations’ AUROC results under the Clean setting. Left: MNIST digit ‘5’ as the inlier data. Right: CIFAR10 ‘automobile’ as the inlier data. We conduct each experiment 3 times with different random initialization, where each plot’s x-axis corresponds to the experiment index. Performance reported in the original paper [33] appears above what we have obtained on average for both datasets.

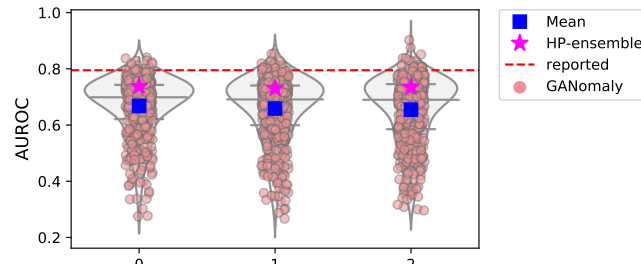


Figure 8: AUROC results with varying HP configurations for the GANomaly algorithm. We utilize the same experimental setting as in [4], with MNIST digit ‘4’ as the outlier class, and rest of the digit classes as inliers (also in Clean setting). The x-axis corresponds to the experiment index among 3 independent runs each with a different random initialization. Performance reported in the original paper [4] appears above what we have obtained on average.

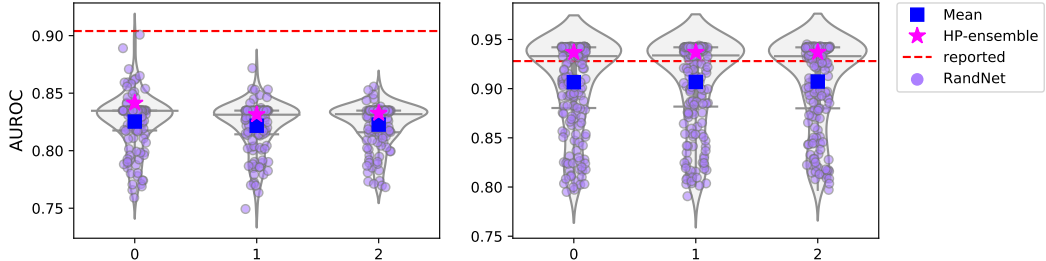


Figure 9: AUROC results with varying HP configurations for the RandNet algorithm. As RandNet implementation contains fully connected layers, we evaluate it only on tabular data under Polluted setting, similar to the experiments in [3]. Left: Thyroid dataset, Right: Cardio dataset. Each plot’s x-axis corresponds to the experiment index for 3 different runs with random initialization.

RandNet are trained with AE for all three kinds of datasets; DeepSVDD is trained with Convolutional AE (LeNet) on image data and AE on tabular data; RDA is trained on AE for MNIST and tabular data, it utilizes Convolutional AE (LeNet) on CIFAR10. If an algorithm is trained with AE as the underlying structure, we define a shared grid of HPs: number of encoder layers, decay rate (the rate of NN width’s shrinkage between current and next encoder layers), dropout rate, train learning rate, etc. Similarly for Convolutional AE, the algorithms apply the same grid of HPs: convolution channels, fully-connected layer dimensions, weight decay, learning rate, etc.

With respect to model-specific HPs, RDA uses λ as a penalty constant for sparsity of the outlier matrix. It also uses `inner_iters` and `iter`, to specify the number of epochs respectively for training an AE and for separating the data into outlier and inlier matrices. For RandNet, we fix the number of ensemble members to 5 due to computational overhead in training high-dimensional image datasets, while [3] uses 50 ensemble members as RandNet is trained on tabular data only. Other model-specific HP descriptions can be found in Sec. A.2 Model HP Descriptions and Grid of Values.

Table 8: Grid of values for the HPs and neural architectures used in experiments.

HPs	AE	LeNet (MNIST)	LeNet (CIFAR10)
Number of encoder layers	[2,3,4,5,6]	[2]	[3]
Decay rate	[1.5,1.75,2,2.25,2.5,2.75,3,3.25]	-	-
Convolution channels	-	[8]	[16]
FC layer dimensions	-	[16,32,64]	[32,64,128]
Dropout rate	[0.0,0.2]	-	-
Weight decay	[0,1e-5]	[0,1e-5,1e-6]	[0,1e-5,1e-6]
Train Learning Rate	[1e-3,1e-4]	[1e-4,1e-5]	[1e-4,1e-5]
NN settings for dataset:			
VanillaAE	AE	AE	AE
DeepSVDD	LeNet (MNIST)	LeNet (CIFAR10)	AE
RDA	AE	LeNet (CIFAR10)	AE
RandNet	AE	AE	AE
Method			
VanillaAE	train iters: [250,500]		
RDA	λ : [1e-1,1e-3,1e-5], iters: [20,30], inner iters: [20,30]		
DeepSVDD	LeakyRelu Slope: [1e-1, 1e-3], pretrain iters: [100,350], pretrain lr: [1e-4], train iters: [250,500]]		
RandNet	pretrain iters: [100], pretrain lr:[1e-4] adaptive sampling rate: [1.0] train iters: [250,500], ens_size = [5]		

For each data point, i-ROBOD provides a score by averaging each individual VanillaAE’s reconstruction error for a data point, thus the training time required for i-ROBOD sums up each VanillaAE’s time. ROBOD speeds up i-ROBOD with fast ensembles across varying NN depths and widths. Table 9 shows the architecture overview for ROBOD. Specifically, the NN depths and widths are set to 8 and 6, representing the implicit ensembles. ROBOD explicitly ensembles over various train iterations, learning rates, dropout rate, weight decay, providing an averaged reconstruction error score for each data point. We also experiment with two subsampling based versions, denoted ROBOD- δ , where $\delta = 0.1$ and 0.5 , respectively. We let ROBOD- δ to train each ensemble member only on 10% or 50% of the training data, and score “out-of-sample” points, i.e. the rest of the (unseen) data points.

Table 9: ROBOD architecture overview

List of HPs	Settings
BatchEnsemble num_models	8 (implicit ensemble over decay rate: [1.5,1.75,2,2.25,2.5,2.75,3,3.25])
num_layers	6 (implicit ensemble over AE-2, AE-4, AE-6,AE-8,AE-10,AE-12)
Train iterations	[250,500]
Train Learning Rate	[1e-3,1e-4]
Dropout rate	[0.0, 0.2]
Weight decay	[0, 1e-5]

A.5.2 Dataset Description

Similar to the experiment settings in our sensitivity analysis, we evaluate the baseline methods and ROBOD on image data (MNIST, CIFAR10) as well as tabular data (Thyroid, Cardio and Lympho). For MNIST, we conduct three sets of experiments; each chooses digit ‘4’, ‘5’, or ‘8’ as the inlier class, respectively. For CIFAR10, we conduct two sets of experiments, with ‘airplane’ (CIFAR10-0) and ‘automobile’ (CIFAR10-1) as the inlier classes. For image data, we employ global contrast normalization to individual images. The inliers are assigned the label 0 and all classes other than the inlier class will be marked with 1, indicating the outlier class. We conduct all experiments under the Polluted setting, where we use all the inlier class points from Pytorch’s train data-split as label 0, and combine them with 10% of points from the outlier classes within the train data-split. The tabular data, Thyroid, Cardio and Lympho, are downloaded from the ODDS repository (available at <http://odds.cs.stonybrook.edu/>, which contain 2.5%, 9.6% and 4.1% outliers, respectively. Similar to image data, the inliers have label 0 and outliers have label 1. Prior to model training, we transform and scale each feature between zero and one using the MinMaxScaler.

A.6 Additional Experiment Results

Fig. 10 is shown to illustrate the regularization effect of parameter sharing in AE-S versus a vanilla AE. (See A.4 for discussion.)

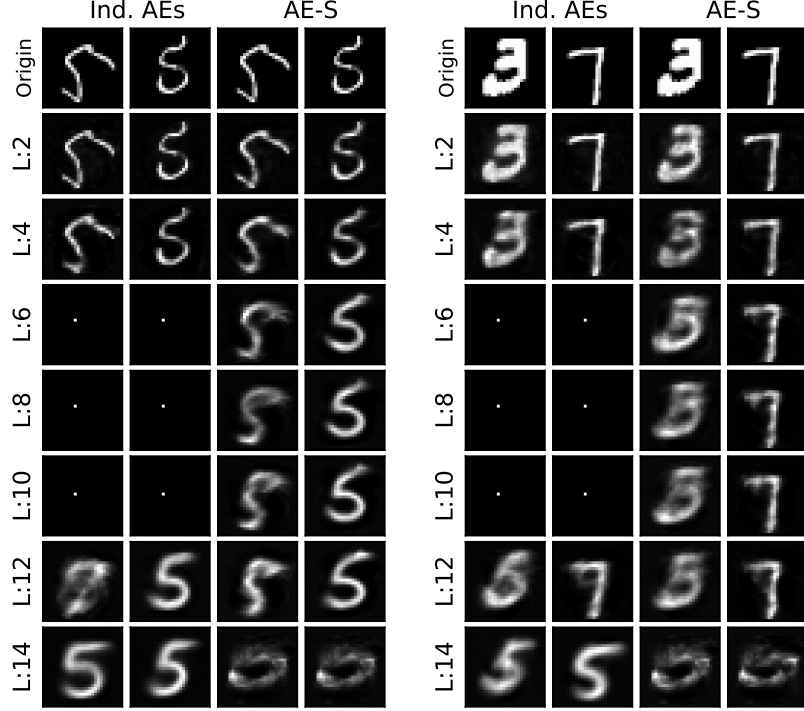


Figure 10: Left: Reconstructed *inlier* class instances (MNIST digit ‘5’), generated by individual AEs vs AE-S structure in ROBOD. Right: Reconstructed *outlier* class instances (MNIST digit ‘3’ and ‘7’) by individual AEs versus AE-S structure. L denotes the number of layers.

Fig. 11 shows the running time (in log scale) vs. AUROC performance of OD methods (symbols) on datasets MNIST-4, MNIST-5, CIFAR-airplane, CIFAR-automobile, Thyroid and Lympho.

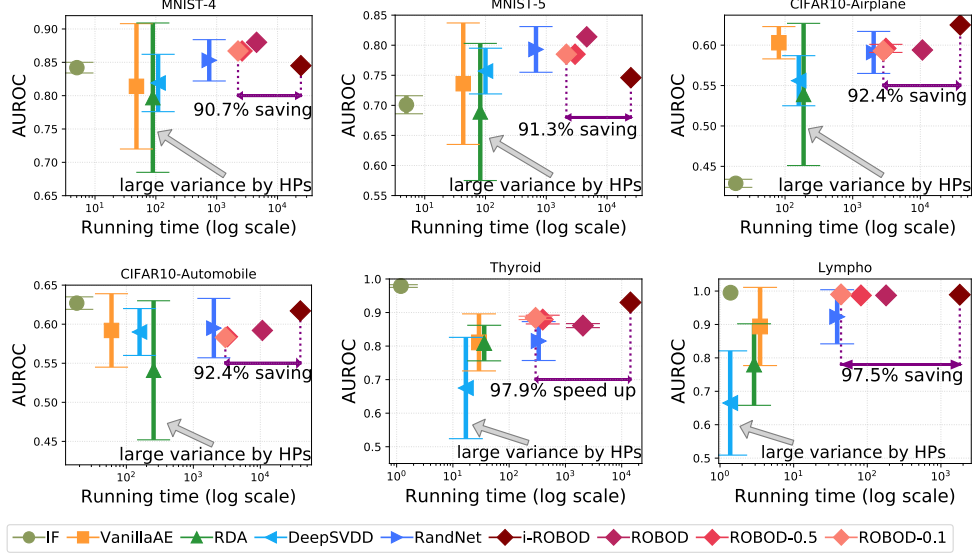


Figure 11: Running time (in log scale) vs. AUROC of OD methods (symbols) on other datasets. Vertical bars depict one (1) stdev across HP config.s. ROBOD often improves detection performance and importantly, provides robust low-variance performance. Sampling based ROBOD reduces running time considerably with small difference in relative performance.